Design considerations for circularly form-birefringent optical fibres

Y. Fujii and C.D. Hussey

Indexing term: *Optical fibres*

Abstract: Single-lobe and multiple-lobe single-mode fibre core structures which are twisted at a uniform rate along the fibre axis are proposed as candidates for achieving very high circular birefringence in optical fibres. The main characteristics of these structures are analysed in general terms using ray optics. These circularly birefringent fibres can give 100% twisting efficiency without any linear birefringence effects. Even with parameters similar to conventional monomode fibres, the maximum obtainable birefringence can be a few rotations/mm.

1 Introduction

Circularly birefringent fibres have a practical importance for optical transmission, for optical sensors and for optical fibre components. Such birefringence in fibres has been realised by mechanically twisting conventional fibres and thereby utilising the elasto-optic effect due to the twist-induced stress [1] or torsion.

Obviously, circular birefringence could also be obtained by the use of a core material which has optical activity or by Faraday rotation. The fourth possibility which we explore in this paper is to utilise the index distribution only.

Many authors have performed theoretical and experimental work on circularly birefringent fibres; for example the twisted fibres using the elasto-optic effect [1, 2], spun fibres [3–5] and fibres with Faraday rotation for sensing purposes [6]. Helical* fibres have been proposed and realised [7, 8] for some time as examples of circularly form-birefringent fibres.

There are now well developed techniques for fabricating fibres with complex structures, which open further possibilities for realising circular form-birefringence in fibres. In this paper we explore such structures and find that if they are twisted in the direction of propagation they are capable of obtaining a much higher circular birefringence than has previously been achieved.

In this paper the necessary considerations to realise such a circularly form-birefringent fibre are treated in general terms using ray optics, and new 'spiral, and 'twisted-cross' fibres are proposed as the most likely candidates for them. The analysis given here gives such parameters as the maximum circular birefringence, the undulation of the guided beam, the extinction and the excitation efficiency in the simplest form as functions both of the fibre dimensions and of the index difference between the core and the cladding.

2 Conditions for circular birefringence

In order to realise a circularly form-birefringent fibre, it is necessary (i) to obtain an imaginary coupling coefficient [1] between the two orthogonal polarisations which is proportional to the twisting rate and (ii) to supress any type of linear birefringence.

Clearly, if a twist is to have any effect on the polarisation of the propagating field it is necessary to introduce some azimuthal inhomogeneity into the core. We shall consider some very large inhomogeneities in the form of single- and multiple-lobe core fibres, a few variations of which are shown in Fig. 1.

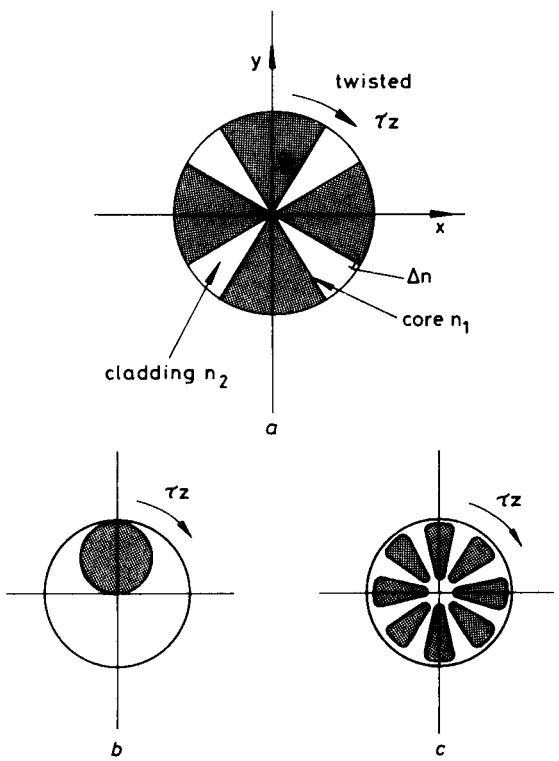

Fig. 1 *Cross section of twisted multicore fibres*
a Four-core lobes ('twisted-cross' fibre),
b One-core lobe ('spiral' fibre)
c Eight-core lobes ('octopus' fibre)

A detailed perturbation analysis for a small aximuthal inhomogeneity of the type in Fig. 1*a* in a step-index monomode fibre is contained in Appendix 8. In this case the maximum coupling coefficient obtainable is found to be $i(\Delta n/n)\tau$, where τ is the twist rate per unit length and $\Delta n/n$ is the relative refractive-index difference between the inhomogeneity and the core refractive index; the coupling coefficient is imaginary as required.

Although perturbation theory can be used to analyse fibres with slightly deformed cores, it is difficult to apply to those structures where the inhomogeneous lobes themselves form the guiding structure. The reasons for this are

* We use the term 'spiral' to distinguish the case where the core offset distance from the axis is approximately equal to the core diameter, we will reserve the term 'helical' for those cases where the offset is much larger [7, 8].

Paper 4751J (E13) received 28th October 1985

The authors are with the Department of Electronic and Information Engineering, The University, Southampton SO9 5NH, United Kingdom. Dr. Fujii is on leave from the Institute of Industrial Science, University of Tokyo, Japan

(i) the coupled power originates from longitudinal total internal reflection, not from transverse reflections due to the index difference, (ii) the index gradient is so large that the mode profile should be entirely changed and (iii) higher modes, not only the two perpendicular modes, are excited at the reflecting boundary.

In the well-confined optical waveguide, the fields are assumed to remain in the waveguide with their profiles unchanged. This affords a physical basis for the 'axiom' [7]: 'if linearly polarised light is launched into a fibre which is bent into a planar curve, then the angle which the polarisation makes with the normal to the plane stays constant'. However, it also holds as long as the twist is slow and, as shown later, the rays in the core are internally reflected at the core-cladding boundary.

To demonstrate that the coupling coefficient is imaginary, let us consider a fibre twisted around the z-axis with twist rate τ per unit length. If the fields are guided with their profile unchanged, then, after a small distance Δz, the two orthogonal fields (locally perpendicular with each other) are expressed, in the co-ordinates fixed at $z = 0$, as

$$E_1(\Delta z) = E_1(0) \cos \tau\Delta z + E_2(0) \sin \tau\Delta z \quad (1)$$

$$E_2(\Delta z) = -E_1(0) \sin \tau\Delta z + E_2(0) \cos \tau\Delta z \quad (2)$$

Thus, we have, automatically, the coupling equations as

$$\frac{dE_1}{dz} = i\kappa_{12} E_2 = \tau E_2 \quad (3)$$

$$\frac{dE_2}{dz} = i\kappa_{21} E_1 = -\tau E_1 \quad (4)$$

Where the coupling coefficients are imaginary as:

$$\kappa_{12} = -i\tau = \kappa_{21}^* \quad (5)$$

The circular birefringence is therefore equal to 2τ.

The twist efficiency, defined as the ratio of the coupling coefficient to the twist rate, is 100% in this case. In comparison, for the elasto-optically twisted fibres [1], the twist efficiency is about 8%, whereas in spun fibres, or in a stack of twisted birefringent plates [9, 10], it is much smaller.

The condition necessary to suppress the linear birefringence is intuitively obtained as follows: (i) if each lobe is uncoupled with the other, then each lobe must not have any linear birefringence. (In this case it is clearly more sensible to consider the single lobe 'spiral' fibre of Fig. 1*b*); and (ii) if the lobes are coupled, the core structure must have at least two equal mirror symmetries perpendicular with each other (this is the case of 'twisted-cross' or 'octopus' fibre [11, 12] see Fig. 1*a* and 1*c*.

3 Analysis by ray optics

As the mechanism of twisting relies on longitudinal total internal reflection, the use of ray optics provides an intuitive and quantitatively excellent [13] basis, both for analysing the twisting structures of Fig. 1, and also for providing general design criteria for their implementation. In ray optics, a propagating mode is represented by a bundle of rays which are totally internally reflected in a zigzag manner between a pair of boundaries, with an angle ψ_m to the boundary when the guide is not twisted. The angle ψ_m must be smaller than the critical angle ψ_c (the configurations and the definitions are summarised in Fig. 2). Using the definitions in Fig. 2, we have

$$\sin \psi_m = \sqrt{1 - (\beta/\beta_1)^2} = \sin \psi_c \sqrt{1 - B} < \sin \psi_c \quad (6)$$

So, the incident angle ψ_m corresponds to a specific value of β i.e. to a specific mode.

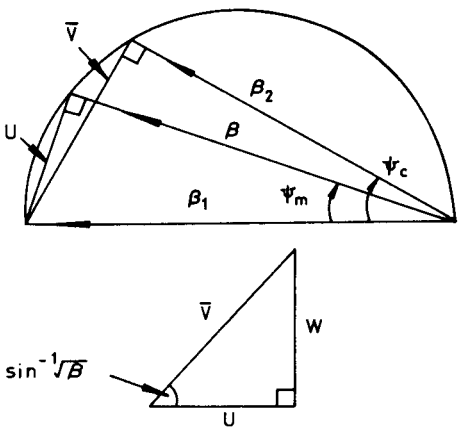

Fig. 2 *Diagram of the propagating-wave vector β and the wave vectors $\beta_1 = k_0 n_1$, $\beta_1 = k_0 n_2$*

k_0 is the wave number in vacuo. $V^2 = \beta_1^2 - \beta_2^2$ $B = (\beta^2 - \beta_2^2)/(\beta_1^2 - \beta_2^2) = W^2/V^2$. The critical angle ψ_c is defined as $\sin \psi_c = V/\beta_1 = \sqrt{2\Delta n/n}$

The boundary between the lobed core and the intermediate cladding is shown schematically in Fig. 3. The totally internally reflected ray is incident from the untwisted section of the guide onto the boundary of the twisted guide with an angle $\psi_\pm$ to the boundary, as

$$\psi_\pm = \psi_m \pm \tau r \quad (7)$$

where the double sign corresponds to the reflections at the

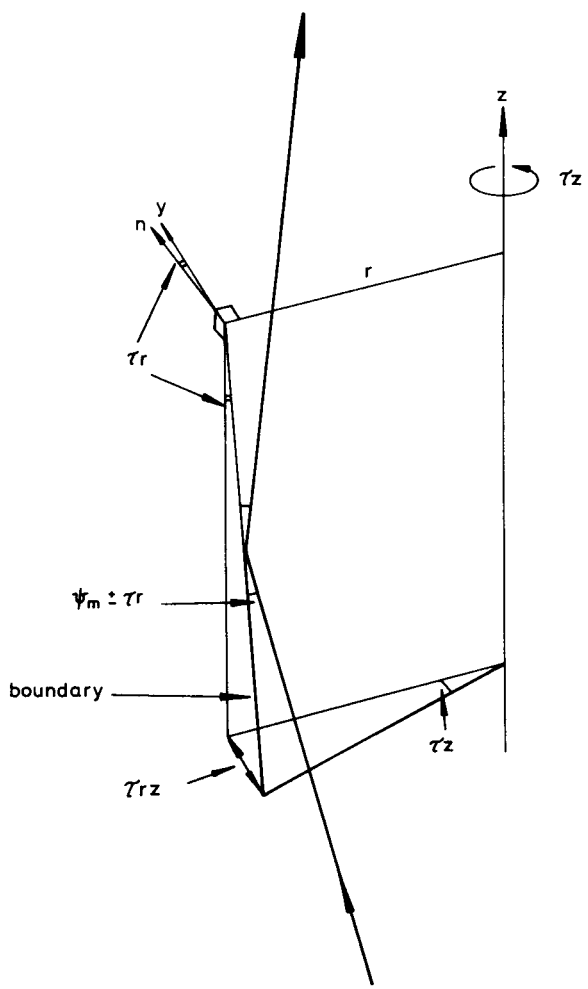

Fig. 3 *Configuration of the boundary between the core lobes and the intermediate cladding*

τ: the twist rate, n: normal to the boundary and r: the radius from the axis of the twist

front and back boundaries. To ensure total internal reflection, the angle $\psi_\pm$ must be smaller than the critical angle ψ_c.

$$\psi_\pm < \psi_c \tag{8}$$

Thus, we have the maximum realisable twist rate as

$$\tau_{max} < (\psi_c - \psi_m)/r_0 \tag{9}$$

where r_0 is the outermost radius of lobes from the twist axis. τ_{max} is the maximum twist rate for which both rays propagate and for which we have 100% twisting efficiency, by twisting at faster rates the twisting efficiency is reduced.

As the incident angles on the twisted boundary ψ_+ do not correspond to any eigenmode of the twisted waveguide, the field is no longer stationary. The field profile contains higher-order modes, but it changes periodically by an inverse of the periods, $\Delta\beta_\pm$ as:

$$\Delta\beta_\pm = |\beta_+ - \beta_-| = 2\beta_1 \tau r \psi_m \tag{10}$$

This equation is obtained from eqn. 7, and the definitions of $\beta_\pm$ are

$$\beta_\pm^2 = \beta_1^2(1 - \psi_\pm^2) \tag{11}$$

The field spread out into the intermediate cladding is mixed up with the field from the neighbouring core. Thus, this component cannot be twisted. This portion of power U_c is estimated as

$$U_c = \frac{e^{-2Wd_x}}{4Wr_e + 1} \tag{12}$$

where W is the decay constant in the cladding, d_x is the half effective thickness of an intermediate cladding, and r_e is the half effective thickness of a core lobe, where the field is assumed to be uniformly distributed.

In 'spiral' fibres, if the axis of twist is in the core lobe, a part of the field cannot be twisted because it sees no reflecting boundary, as shown by the light area in Fig. 4*a*.

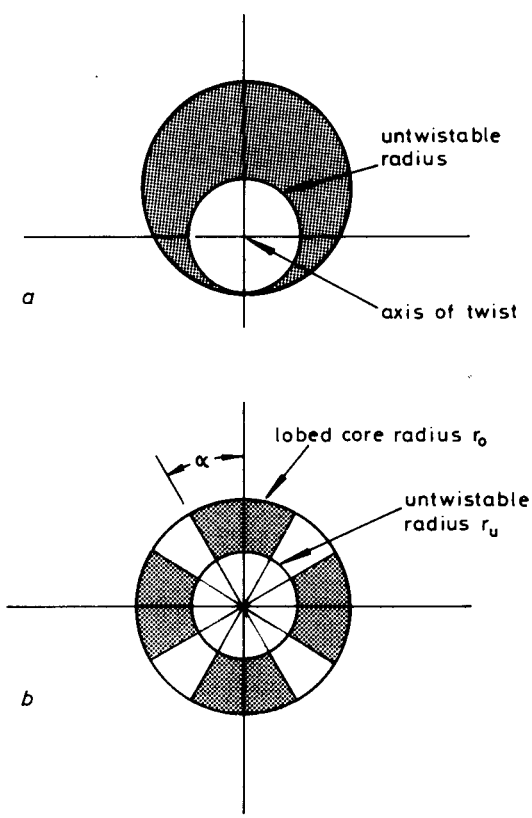

Fig. 4 *Cross-sections of (a) 'spiral' fibres and (b) 'twisted cross' fibres*
Only the dark area can be used for the twisted guide

In 'twisted-cross' fibres, the field penetrates into the cladding by W^{-1}. Thus the fields of the neighbouring lobe are mixed up and the fields cannot be twisted. This 'untwistable' radius, r_u may be estimated simply

$$r_u = \frac{1}{W\left(\frac{\pi}{4} - \alpha\right)} < r_0 \tag{13}$$

where α is the half angle of the lobe (Fig. 4*b*). Thus rotation may only be obtained in the dark area in Fig. 4*b*.

4 Numerical examples and discussion

Numerical examples of the characteristics of 'twisted-cross' fibres are calculated using the preceding relations. Field profiles are roughly estimated as if each lobe is itself a monomode fibre. Because the field distribution of the rectangular dielectric waveguide is very similar to that of the step-index fibre [14], the propagation constant is estimated from the results for circular fibres [15].

The numerical examples are given for 'twisted-cross' fibres, however, the methods can also be applied to other form-birefringent fibres, including the 'spiral' and octopus' fibres as in Fig. 1.

Fig. 5 shows the optimum lobed-core radius to obtain

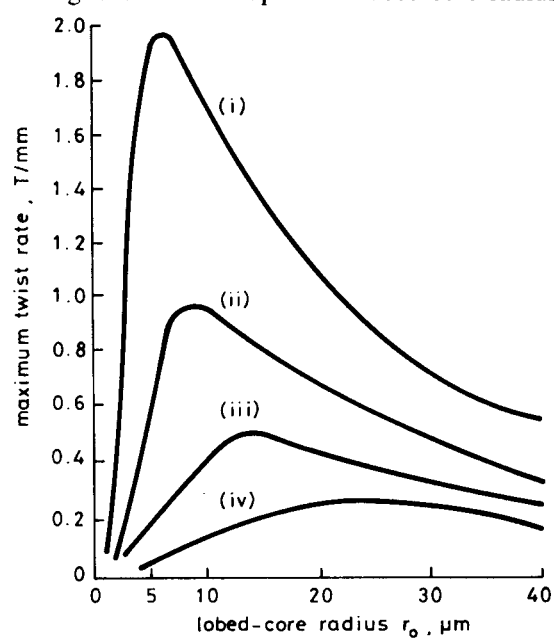

Fig. 5 *Maximum obtainable twist rate as a function of the lobed-core radius and the index difference*
$\alpha = 30°$
(i) $\frac{\Delta n}{n} = 0.016$
(ii) $= 0.008$
(iii) $= 0.004$
(iv) $= 0.002$

the maximum twist rate. The optimum appears from a compromise between poor capability of field confinement, at small radius, and the spilling out of field at the outermost radius, where the peripheral twisting speed is high. The optimum radius decreases approximately as $(\Delta n/n)^{-1/2}$.

The 'undulation length' at the maximum value of the twist rate is shown in Fig. 6. This phenomenon is very similar to the undulation of a beam obliquely incident to a graded-index medium. The 'undulation length' is inversely proportional to the twist rate, as shown in eqn. 10; thus we will have longer values than that shown in Fig. 6, if the twist is slow.

The untwistable power, estimated by eqn. 12, is shown in Fig. 7. Of course it can be much improved by increasing the index difference. Remarkably, we have an untwistable power of −25 dB at the optimum twist rate for all values of the index difference.

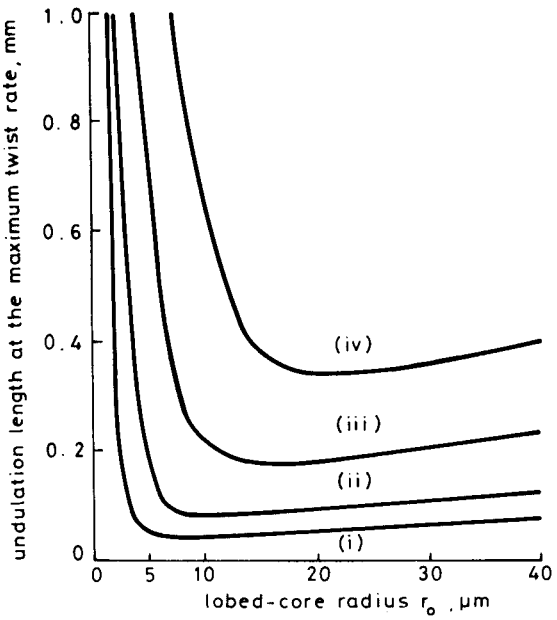

Fig. 6 *Undulation length of the field profile at the maximum twist rate as a function of the core radius and the index difference*

$\alpha = 30°$

(i) $\frac{\Delta n}{n} = 0.016$
(ii) $= 0.008$
(iii) $= 0.004$
(iv) $= 0.002$

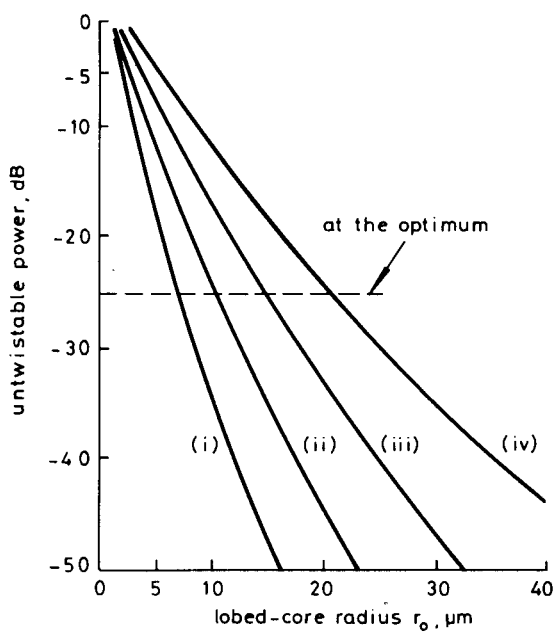

Fig. 7 *Ratio of the untwistable power to the guided power as a function of the core radius and the index difference*

$\alpha = 30°$

(i) $\frac{\Delta n}{n} = 0.016$
(ii) $= 0.008$
(iii) $= 0.004$
(iv) $= 0.002$

In Fig. 8 the untwistable radius is estimated by eqn. 13. In the area where $r_u > r_0$, the twisting of the field cannot be achieved. Thus, the excitation from an incident beam, assumed to be uniform within the outermost radius r_0, is effectively done in the dark area in Fig. 4*b*. The simplest estimation of the excitation efficiency (i.e. the ratio of the dark area to the full area within r_0) is shown in Fig. 9.

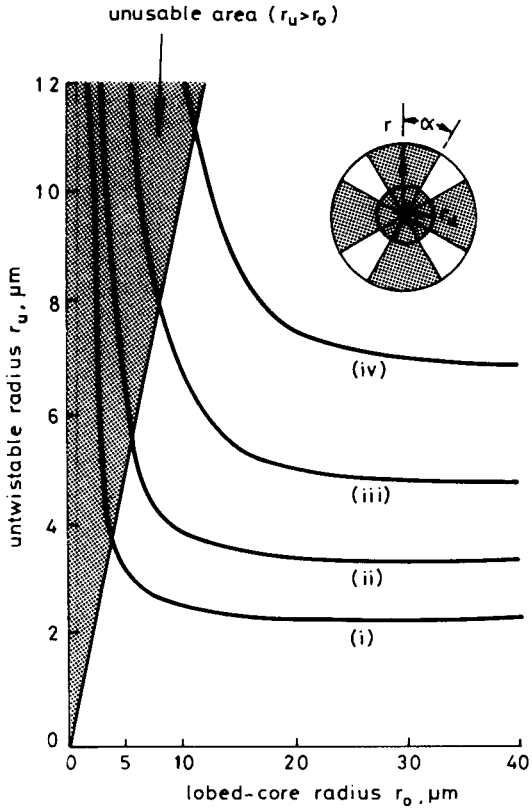

Fig. 8 *Untwistable radius r_u, calculated by using eqn. 13. No twist of the field will be achieved in the region where r_u exceeds the outermost radius r_0*

$\alpha = 30°$

(i) $\frac{\Delta n}{n} = 0.016$
(ii) $= 0.008$
(iii) $= 0.004$
(iv) $= 0.002$

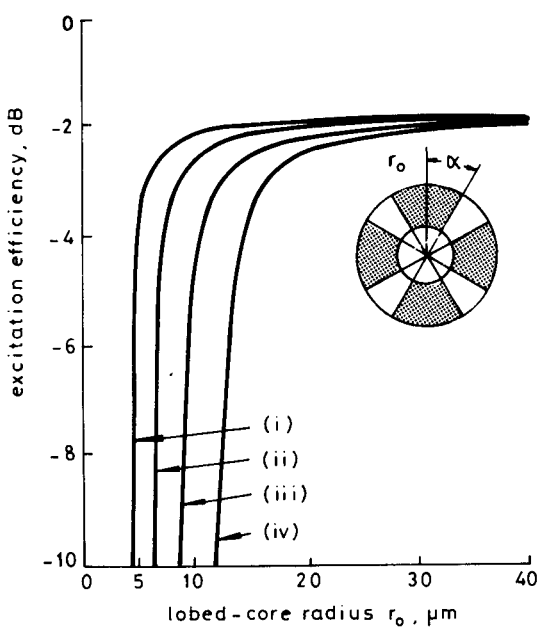

Fig. 9 *Excitation efficiency assuming uniform excitation within the outermost radius r_0*

$\alpha = 30°$

(i) $\frac{\Delta n}{n} = 0.016$
(ii) $= 0.008$
(iii) $= 0.004$
(iv) $= 0.002$

The maximum twist rate, the untwistable power and the excitation efficiency are estimated as a function of the half-lobe angle α for the optimum outermost radius, r_0, for each value of the index difference ($\Delta n/n$) (Fig. 10). The excitation efficiency and the untwistable power remain approximately the same, irrespective of the value of ($\Delta n/n$).

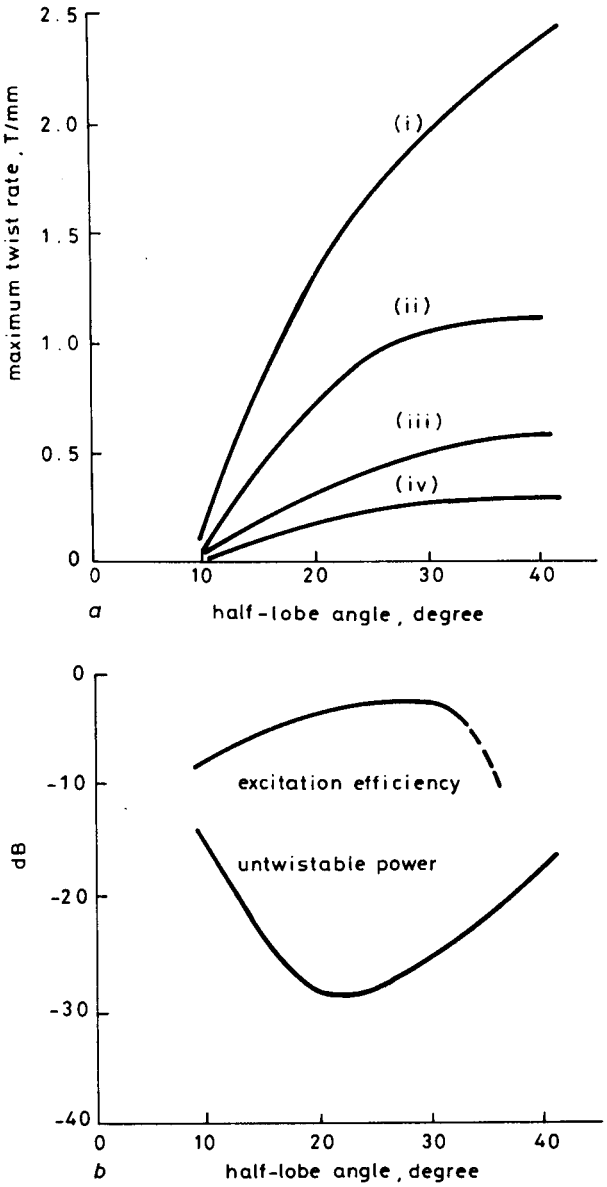

Fig. 10 *Maximum twist rate (a) and excitation efficiency and untwistable power (b) as a function of the half-lobe angle, at the optimum value of r_0 to $\Delta n/n$ for the maximum twist rate*

(i) $\frac{\Delta n}{n} = 0.016$ ($r_0 = 7$ μm)
(ii) $= 0.008$ ($= 10$ μm)
(iii) $= 0.004$ ($= 15$ μm)
(iv) $= 0.002$ ($= 20$ μm)

From these results, we may say that $\alpha = 30°$ is the optimum for every practical value of $\Delta n/n$.

The excitation of these fibres from conventional HE_{11}-mode fibres, is a problem of a trade-off between the untwistable power (i.e. extinction) and the excitation efficiency. A tapered coupler might be devised, but it would be difficult to fabricate.

To improve the confinement, it is desirable that the index of the intermediate cladding should be chosen to be less than the surrounding cladding, and that the portion of the lobed cores within the untwistable radius should be removed.

As a result, we may have a fibre configuration which has a 'clover-leaf' lobe structure (Fig. 11). Although the numerical values are shown in Fig. 11 only as an example, we can design with other parameters.

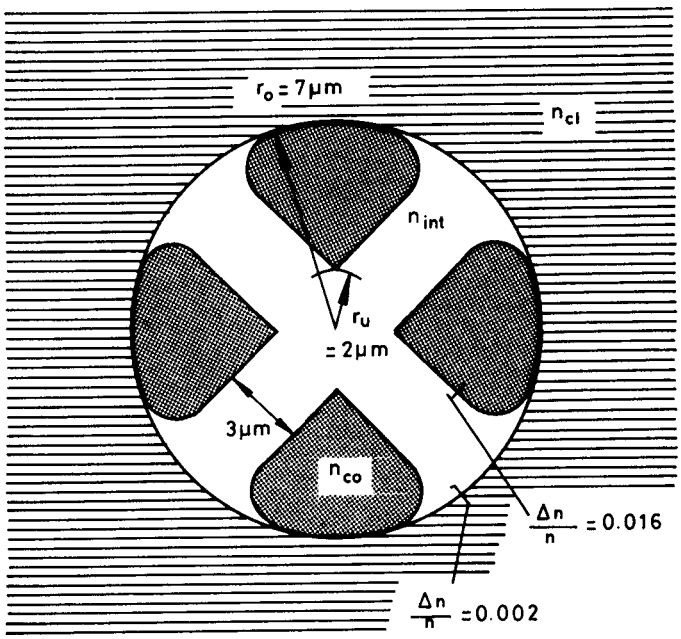

Fig. 11 *Example of the optimum design of a clover-leaf circularly birefringent fibre*

$\tau = 2T/mm$
$n_{co} > n_{cl} > n_{int}$

Almost all the parameters shown here are applicable to the 'spiral' or 'octopus' fibres with little amendments.

If each lobe is itself regarded as a monomode fibre, then the normalised frequency V, which corresponds to the optimum twist rate, is about 3.5 for each $\Delta n/n$.

This means that the design conditions obtained here for circularly form-birefringent fibres may be readily satisfied with the conventional parameters of monomode fibres.

The 'spiral fibre' should be the simplest to implement. The 'twisted-cross' fibres are more complex, but because they have a symmetrical structure, it seems easier to remove any residual linear birefringence which may be duce to the deformation of core, or to the elasto-optic effect. The influence of the elasto-optic effect [1] and of the Faraday rotation, if they exist, may be linearly added, as long as these effects are small [7].

For more detailled discussion, it is indispensable to calculate the exact field profile.

5 Conclusion

We give the principles for designing circularly form-birefringent fibres and, as examples, we propose the 'spiral' and 'twisted-cross' or 'clover-leaf' fibres. The multicore fibres have been analysed and also fabricated by many [11, 12, 16]. We believe, therefore, that it should be relatively easy to realise circularly form-birefringent fibres which exhibit reasonable characteristics.

These fibres should be effective in obtaining high circular birefringence because they have 100% twisting efficiency.

6 Acknowledgments

The authors wish to express thanks to Professor Gambling and to their colleagues at Southampton for providing a stimulating research atmosphere.

7 References

1 ULRICH, R., and SIMON, A.: 'Polarisation optics of twisted single mode fibers', *Appl. Opt.*, 1979, **18**, (13), pp. 2241–2251
2 MONERIE, M., and JEUNHOMME, L.: 'Polarisation mode coupling in long single-mode fibres', *Opt. & Quantum Electron.*, 1980, **12**, pp. 449–461
3 BARLOW, A.J., and PAYNE, D.N.: 'Polarisation maintenance in circularly birefringent fibres', *Electron. Lett.*, 1981, **7**, (11), pp. 388–389
4 BARLOW, A.J., RAMSKOV-HANSEN, J.J., and PAYNE, D.N.: 'Birefringence and polarisation mode-dispersion in spun single-mode fibres', *Appl. Opt.*, 1981, **20**, (17), pp. 2962–2968
5 BARLOW, A.J., PAYNE, D.N., HADLEY, M.R., and MANSFIELD, R.J.: 'Production of single-mode fibres with negligible intrinsic birefringence and polarisation mode dispersion', *Electron. Lett.*, 1981, **17**, (20), pp. 725–726
6 RASHLEIGH, S.C., and ULRICH, R.: 'Magneto-optic current sensing with birefringent fibres', *Appl. Phys. Lett.*, 1979, **34**, (11), pp. 768–770
7 ROSS, J.N.: 'The rotation of the polarisation in low birefringence monomode optical fibres due to geometric effects', *Opt. & Quantum Electron.*, 1984, **16**, pp. 455–461
8 PAPP, A., and HARMS, H.: 'Polarisation optics of liquid core optical fibres', *Appl. Opt.*, 1977, **16**, (5), pp. 1315–1319
9 STOKES, A.R.: 'The theory of the optical properties of inhomogeneous materials' Chap 4, in 'Birefringence and Optical Rotation' (E. & F.N. Spon Ltd), 1963
10 MCINTYRE, P., and SNYDER, A.W.: 'Light propagation in twisted anisotropic media: Application to photoreceptor', *J. Opt. Soc. Am.*, 1978, **G8**, (2), pp. 149–157
11 ROMANIUK, R.S., and DOROSZ, J.: 'Coupled/noncoupled wave transmission in long-length of multicore optical fibres', ECOC '84, Stuttgart, W. Germany, 3–6th Sept., 1984, 11A6
12 ROMANIUK, R.S., and DOROSZ, J.: 'A family of multicore optical fibre based sensors and instrumentation systems', J.OFS '84, Stuttgart, W. Germany, 5–7th Sept., 1984, p. 22
13 ADAMS, M.J.: 'An introduction to optical waveguides', (Wiley, 1981)
14 GOELL, J.E.: 'A circular harmonic computer analysis of rectangular dielectric waveguides', *Bell. Syst. Tech. J.* 1969, **48**, pp. 2133–2160
15 GLOGE, D.: 'Weakly guiding fibres', *Appl. Opt.*, 1971, **10**, pp. 2252–2258
16 KITAYAMA, K., SEIKAI, S., and UCHIDA, N.: 'Polarisation-maintaining single-mode fibre with azimuthally inhomogeneous index profile', *Electron. Let.*, 1981, **17**, (12), pp. 419–420
17 SNYDER, A.W., and YOUNG, W.R.: 'Modes of optical waveguides', *J. Opt. Soc. Am.*, 1978, **68**, (3), pp. 297–309

8 Appendix: Analysis of the twisted-cross fibre by the coupled-mode equations

8.1 Introduction

The coupled-mode formalism is a very effective tool for calculating the birefringences due to small changes of the index profile. This formalism is applicable to the analysis of the 'twisted-cross' fibre (Fig. 1*a*) when the index difference is very small and the field profile is almost uniform.

8.2 Generalised coupling coefficient to a line integral

The coupling coefficient between two electric fields $\boldsymbol{e}$ and $\tilde{\boldsymbol{e}}$ is given by Snyder and Young [17] and it is generalised to include the three-dimensional index gradient as

$$\kappa = \frac{\int_A \tilde{\boldsymbol{e}} \cdot (\nabla(\boldsymbol{e} \cdot \nabla \ln \varepsilon))\, dA}{2\beta \int_A \tilde{\boldsymbol{e}} \cdot \boldsymbol{e}\, dA} \tag{14}$$

where $\tilde{\boldsymbol{e}}$ is the standard distribution, and $\boldsymbol{e}$ is the perturbed distribution but is assumed to be expandable by $\tilde{\boldsymbol{e}}$.

This equation holds for the coupling problems including the index profile and its gradient. β is an averaged propagation constant between two modes.

In practical cases, the configuration of the index distribution is made by abrupt step changes of index. In these cases, the numerator in eqn. 14 has a nonzero value only on the surface of the step index change, so that it is convenient to convert it into an integral for such surfaces only. The integrand of the numerator in eqn. 14 can be rewritten in terms of the local normal and tangential co-ordinates, n and t, as shown in Fig. 12, as

$$\tilde{\boldsymbol{e}} \cdot \nabla(\boldsymbol{e} \cdot \nabla \ln \varepsilon) = \tilde{e}_n \frac{\partial^2 \ln \varepsilon}{\partial n^2} e_n + \tilde{e}_n \frac{\partial \ln \varepsilon}{\partial n} \frac{\partial e_n}{\partial n} + \tilde{e}_t \frac{\partial \ln \varepsilon}{\partial n} \frac{\partial e_n}{\partial t} \tag{15}$$

where the third term in the right-hand side is negligible because e_n does not have an abrupt change at the surface.

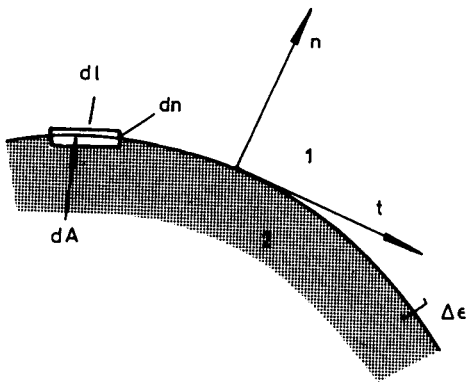

Fig. 12 *Configuration of the surface of a step-index change*

Integrating eqn. 15 by parts locally on the normal axis n, and summing up for the whole cross-section, we get

$$-\int_A \frac{\partial \tilde{e}_n}{\partial n} \frac{\partial \ln \varepsilon}{\partial n} e_n\, dA = -\oint \frac{\partial \tilde{e}_n}{\partial n} \frac{\Delta \varepsilon}{\varepsilon} e_n\, dl \tag{16}$$

The second term is obtained by converting the small area dA to $dndl$. When we then integrate by dn, we assume that the field parameter $e_n\, \partial \tilde{e}_n/\partial n$ is continuous on this surface, and we also rely on the fact that $\partial \ln \varepsilon/\partial n$ has a nonzero value only on the surface of the step-index change. Then, the coupling coefficient κ is given by

$$\kappa = \frac{-\int \frac{\partial \tilde{e}_n}{\partial n} \frac{\Delta \varepsilon}{\varepsilon} e_n\, dl}{2\beta \int_A \tilde{\boldsymbol{e}} \boldsymbol{e}\, dA} \tag{17}$$

8.3 Application to twisted-cross fibres

Consider fibres with core structure as shown in Fig. 1*a*. The core consists of lobes with a certain index interlaced with those of a smaller index. This structure is twisted uniformly along the z-axis by τz. Apparently, this structure (Fig. 1) has no linear birefringence. The normal of the surface of step index change is shown in Fig. 3, and thus

$$\frac{\partial}{\partial n} = \frac{dy}{dn} \frac{\partial}{\partial y} + \frac{dz}{dn} \frac{\partial}{\partial z} \tag{18}$$

Assume that the index difference $\Delta\varepsilon$ is much smaller than the index difference between the core and the cladding, and that the test fields are two HE_{11} modes linearly polarised in the x- and y-directions.

On the surface, the fields normal to the surface are:

$$\tilde{e}_n = E_y J(r) e^{-i\beta z} \sin \alpha \tag{19}$$

$$e_n = E_x J(r) e^{-i\beta z} \cos \alpha \tag{20}$$

where $J(r)$ is the radial field distribution. Thus, using eqn. 18 and the relation in Fig. 3

$$\frac{\partial \tilde{e}_n}{\partial n} = \sin \alpha \left[\frac{\partial J}{\partial y} \cos \tau r + (-i\beta) J \sin \tau r \right] e^{-i\beta z} \tag{21}$$

The first term in the right-hand side can be ignored as the field is almost uniform. Summing up the eight radial surfaces (Fig. 1), the coupling coefficient κ is given by

$$\kappa = \frac{8(\sin\alpha\cos\alpha)(i\beta)\tau\dfrac{\Delta\varepsilon}{\varepsilon}\displaystyle\int_0^{r_0} J^2 r\,dr}{2\beta\cdot 2\pi\displaystyle\int_0^{r_0} J^2 r dr} = \frac{\sin 2\alpha}{\pi}\frac{\Delta\varepsilon}{\varepsilon}\tau i \quad (22)$$

where r_0 is the radius of the core.

It should be noted that the derivation to the tilted normal is essential to obtain the imaginary coupling coefficient. The eqn. 22 is obtained regardless of the field distribution.

The maximum value of κ for the above case, is obtained at $\alpha = 45°$. By increasing the number of lobes, κ increases, but it saturates to

$$\kappa = (\tfrac{1}{2})\cdot(\Delta\varepsilon/\varepsilon)\cdot\tau i \quad (23)$$

for an infinite number of lobes.

8.4 Conclusion

The coupling coefficient obtained is very small. The twist efficiency is of the order of $\Delta\varepsilon/\varepsilon(= 2\Delta n/n)$. This is because no confinement in the lobed cores is assumed, and because only small amounts of reflection from the small index difference $\Delta\varepsilon/\varepsilon$ are utilised for coupling.